2017

Thermo-mechanical modeling and parametric analysis of lithium-ion battery

Abhishek Sarkar
Iowa State University

Thermo-mechanical modeling and parametric analysis of lithium-ion battery

by

Abhishek Sarkar

A thesis submitted to the graduate faculty

in partial fulfillment of the requirements for the degree of

MASTER OF SCIENCE

Major: Mechanical Engineering

Program of Study Committee:
Abhijit Chandra, Co-Major Professor
Pranav Shrotriya, Co-Major Professor
Steve W. Martin

The student author and the program of study committee are solely responsible for the content of this thesis. The Graduate College will ensure this thesis is globally accessible and will not permit alterations after a degree is conferred.

Iowa State University

Ames, Iowa

2017

TABLE OF CONTENTS

LIST OF FIGURES

LIST OF TABLES

ACKNOWLEDGEMENTS

I sincerely acknowledge the guidance provided by my advisors, Prof. Abhijit Chandra and Prof. Pranav Shrotriya, in the completion of the project. I would like to thank them for providing me with resources, literature and solving even the smallest doubts during this project. They have been excellent mentors and always supported me through all the downfalls and triumphs in the duration of the project. I would like to thank Prof. Steve Martin for being a part of my Master's and PhD committee. He has been extremely supporting towards joining my committee and provided excellent advice towards improvement of the data representation.

I thank Prof. Michael Olsen for teaching me Transport Phenomena and being a part of my PhD committee. His excellent teaching has been immensely helpful during the setup of the mathematical formulation for this project. I thank Prof. Pranav Shrotriya for teaching me Mechanics of Solids and Material Selection, which have been a crucial part of this project. I would like to thank Prof. Ashraf Bastawros, Prof. Richard LeSar and Prof. Paul Durbin for teaching me Fracture Mechanics, Behavior of Materials and Computational Fluid Dynamics respectively. Without their teaching and guidance this project could not be completed. I thank the immense resources provided by Iowa State University in fulfilment of the literature review and data collection necessary for this project.

I would like to thank my father for providing me with technical advice and counselling during difficult phases of research and my mother for her support and affectionate care. Finally, I thank my family for providing me with the moral support to strive through my research and take it towards completion.

ABSTRACT

Lithium-ion battery electrodes tend to fracture due to extensive mechanical stress and/or thermally fail by due to overheating. In our present research, we have studied the mechanical and thermal aspect of lithium battery electrodes. Two significant tasks were performed for this project. First, a numerical model was developed for analyzing the crack propagation during lithiation of crystalline silicon. We investigated the influence of mechanical properties of lithiated silicon on the fracture of silicon nanoparticles during lithiation. A chemo-mechanical model was used to determine the lithium distribution and associated stress states during lithiation. The concentration gradient of lithium and an elastic-plastic material response was utilized to determine the stress distribution. The stress distribution was utilized to determine the crack driving forces for radial crack propagation. The crack driving forces were computed for different mechanical response of lithiated silicon. The results showed lower modulus of lithiated silicon made the particle susceptible to fracture, and were validated from prior experiments. These results conclude that accurate mechanical characterization of lithiated silicon is necessary to model the fracture response of silicon particles and improving the mechanical properties will suppress crack growth in a silicon nanoparticle electrode during charging. The second work was based on a thermal parametric analysis of lithium battery electrode materials. Different electrode materials were tested for their thermal performance and life. A material selection analysis was performed based on a multiscale thermo-chemical model. The heat generation associated with lithium transport and mechanical deformation was computed based on polarization, entropic and joule heating. The formulation for the heat generation and dissipation were used to create a set of four material indices that categorize the electrode materials based on their thermal performance and ability to prevent runaway under condition of excess loading. The results predicted that lithium ferrous phosphate and silicon are the best cathode and anode materials, respectively. Heat generation by different materials

was validated against past experimental data. We conclude that at high charging rates the polarization heat generation becomes dominant. We believe that particle size optimization and chemical structure modifications could be plausible options for improving thermal performance of electrode materials.

CHAPTER 1. INTRODUCTION

Lithium ion battery systems is the leading technology in the field of energy storage. Lithium ion Batteries (LIBs) are the leading source of energy storage in the electronic and electric vehicle industry (Armand & Tarascon, 2001). These batteries have a high specific energy density with a long service life. Due to high reusability and energy density compared to other rechargeable batteries, the lithium ion batteries are a favorable power option in electronic and automobile industries.

Lithium-ion Battery

A lithium ion battery works on the principle of electrochemical ion transfer due to a driving potential difference between the electrodes. A galvanic cell has two electrodes; the anode is the negative electrode and the cathode is the positive electrode. The cell runs due to an electrochemical potential difference between the anodic and cathodic materials. An electrolytic solution; generally, the same salt solution as the ions transferred submerges the electrodes providing a pathway for the ions to transfer.

Working Principle

A basic Li-ion battery cell comprises of: a current collector, a negative electrode (anode), a separator, a positive electrode (cathode), and another current collector. The material and microstructures of electrodes and separators vary widely. The materials being used in today's Li-ion batteries include a graphite, silicon, and titanium oxide for negative electrode, $LiMO_y$, where the metal oxide (MO_y) can be manganese oxide, ferrous phosphate, cobalt oxide, etc. A polymeric separator is used to prevent short circuit due to direct contact between electrodes and are made of polypropylene or similar polymers. The entire battery is immersed in the electrolyte made of lithium salts like lithium hexafluorophosphate, lithium hexafluoroarsenate monohydrate, lithium triflate, etc. The electrolyte conducts the Li ion from the

anode to the cathode during discharging cycle and vice-versa during charging as shown in the following reaction.

$$Li_{1-x}MO_y + xLi^+ + xe^- \xrightarrow{cathode} LiMO_y$$

$$Li_xC_6 \xrightarrow{anode} xLi^+ + xe^- + 6C$$

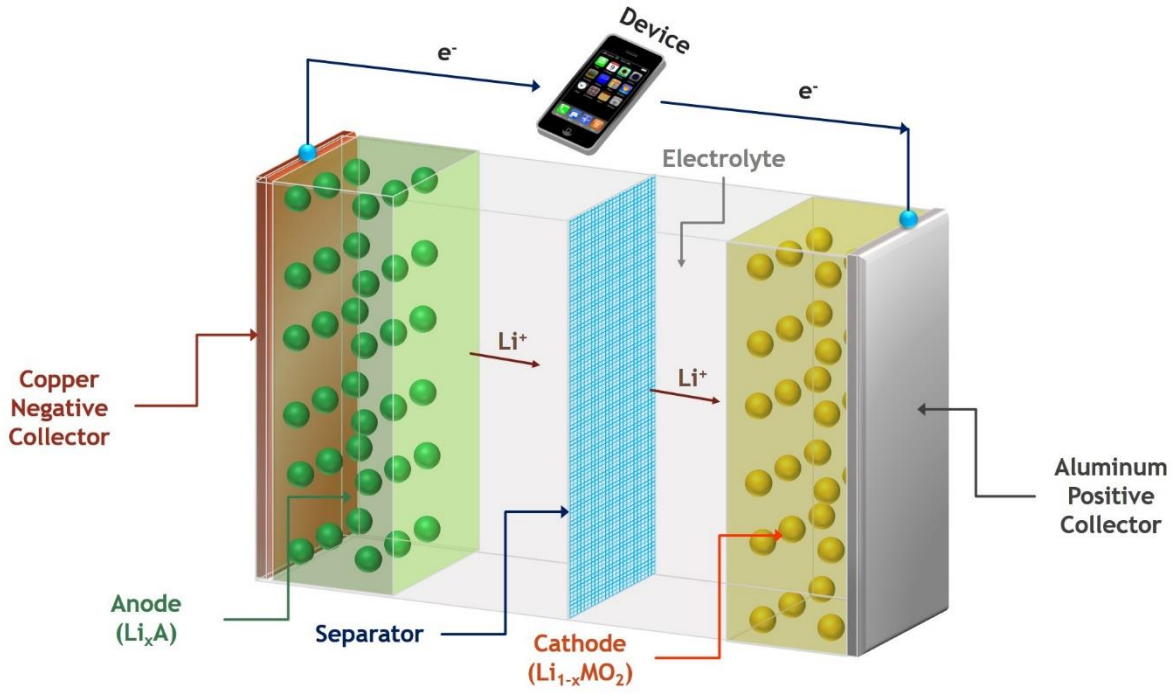

Figure 1. Lithium ion Battery Representation. Li ion and electron transfer circuit diagram with porous electrode representation for lithium metal oxide battery during discharge.

The Figure 1 gives the 3D representation of a Li-ion battery. During charging, the electrons flow into the anode and the Li+ ion also flows towards the anode to bond with the graphite (reduction) by absorbing the electron. The Li+ ion is provided by the $LiMO_y$, which oxidizes as it releases Li+ and electron. The opposite reaction occurs during discharge.

Advancements

Since the development of first commercial lithium-ion batteries by Sony in 1991, there has been paramount research and development related to this battery sector. These batteries were made with graphite anode and a lithium transition metal oxide as cathode (Whittingham, 2004). Rigorous experimental and theoretical study have allowed the evolution and utilization

of better electrode materials, which show higher energy density, longer cycle life, and safer operation (Ellis, Lee, & Nazar, 2010). Recent developments have focused the work on silicon as anode material for the battery systems. Especially with the onset of nanotechnology, silicon nanosphere and nanowire show extreme energy storage capacity (around 4200 mAh/g for $Li_{15}Si_4$). This high-energy storage capacity of silicon occurs due to its ability to expand to ~ 300% of its volume during lithiation. The accommodation of such large volume expansions results in deteriorating tensile and compressive hoop stresses in the electrode particle causing its capacity to fade over multiple cycling (Chang, et al., 2014).

Advantages

There are many advantages of using a li-ion battery.

- Lithium-ion batteries have much greater energy density than other battery sources. A commercial lithium ion battery has an energy density > 200 W-h/kg with a discharge efficiency as high as 95 %. This allows for longer usage time between charges.
- Lithium-ion batteries have a much lower rate of self-discharge than other rechargeable cells such as Ni-Cd and NiMH batteries. This means that the lithium-ion batteries kept stagnant do not lose their charge quickly.
- Lithium-ion batteries do not require maintenance to ensure their performance. They can have a life duration of 10-15 years (2000-4000 operating cycles) before failure.

Drawbacks

However, like other modern day technology, with advantages come some disadvantages. Lithium-ion batteries have certain drawbacks which demands for careful design of these batteries.

- Lithium-ion batteries are not as robust because lithium is highly reactive metal. They require protection from being over charged and discharged and need to have the current maintained within safe limits.
- Lithium-ion batteries have a tendency to age as they are used over multiple cycles. As these batteries age, they start losing their capacity and can store lesser power. Therefore, it is advised to partially charge lithium batteries to improve their energy storage capacity.
- Lithium-ion batteries are about 40% costlier to manufacture than Nickel cadmium cells. This is a major factor when considering their use in mass production.
- Lithium-ion batteries have a tendency of over-heating and getting thermally instable due to overcharging. This caused several incidents of fire and fatality in the past decade.

In the past 5 years, two incidents of battery fire have surfaced resulting from overcharging of lithium ion battery. In Jan-7 2013, fire erupted in a Boeing 787 Dreamliner aircraft when the li-ion batteries got overheated (Irfan, 2014). After the fire was extinguished, the fire fighters found that the batteries were still heating and were about to rekindle the fire. A similar incident occurred in October 2016, when Samsung released its latest model of smartphone, Galaxy Note7. Many incidents across the globe were reported of the phone getting overheated and catching fire. This caused several injuries and burn cases. Samsung recently revealed that the batteries were the cause of the fire due to overheating (Moynihan, 2017).

Current Work

Despite having several advantages in terms of mechanical reliability and high energy storage efficiency, li-ion batteries are prone to thermal runaway leading to overheating and mechanical failure due to fracture. It is essential to study the reasons for failures of lithium-ion batteries and to develop the models for evaluations of the mechanical and thermal parameters

for improvement of future generation of lithium-ion batteries. It is important to setup a selection criteria to choose and compare new electrode materials for lithium batteries and compare them to existing materials. The project was divided into two sections. The first work was based on understanding the fracture characteristics of lithiated silicon during first charge cycle. The second work presented a set of material indices derived from a thermo-chemical model of battery electrode to parametrize three cathode and anode materials based on their thermal performance.

In the first work, we reported the influence of mechanical response on stress and fracture response of nanoparticles during lithiation. Stress fields associated with lithiation of Si nanoparticle were modeled using reaction driven diffusion equation. Calculated stress fields were utilized to determine the driving forces for radial crack in the nanoparticle. Mechanical response of crystalline (c) silicon was modeled as an elastic material while amorphous (a) silicon lithiated mechanical response was modeled as an elastic perfectly plastic material. Numerical predictions were compared to TEM imaging results (Liu, et al., 2012), in order to validate the modelling assumptions. Model predictions were used to identify the critical particle radius for fracture and identify a mechanism to improve the failure performance of the battery.

The second work was based on a thermal parametric analysis of li-ion electrode materials. This analysis took the concentration profile from the elasto-plastic DIS model to estimate three heating sources, i.e. polarization, entropic and joule. The heat of mixing is not considered as the battery was under constant charge-discharge cycling and the magnitude of this source was found to be couple of order smaller than other sources. Four indices were created, of which former three compared the materials' performance for each heating source and the latter was based on the heat dissipation characteristic. It was found that lithium ferrous phosphate and silicon had excellent thermal performance and the former was validated against prior experimental data.

CHAPTER 2. LITERATURE REVIEW

Lithium ion batteries have been a sensational topic for research for over two decades. Since the development and use of rechargeable battery systems for electronic and automotive applications, lithium ion battery has become popular. As compared to other rechargeable batteries, like Ni-Cd or NiMH, lithium ion batteries have a larger energy storage capacity, longer service life and higher energy density (making them portable). Several materials have been considered and tested to be candidate electrodes for lithium battery. The electrode material for lithium batteries started with anode as graphite and cathode as lithium cobalt oxide (Armand & Tarascon, 2001). However, cobalt oxide had several drawbacks including lower thermal stability (Joachin, Kaun, Zaghib, & Prakash, 2009) and higher toxicity, which lead to the prominent use of manganese oxide as cathode material. The search for new materials and their selection made the requirement of an electrochemical model explaining the current voltage profile of the battery during cycles important.

One of the early notable work was done by Doyle et al (1993) (Doyle, Fuller and Newman 1993). Doyle and Newman developed a model for electrochemical transport of species in a lithium battery using concentrated solution theory. Their model used the Nernst-Planck equation combined with electrical charge balance and Butler-Volmer kinetic equation for the electrode surface. The entire electrode was represented by a representative particle submerged in the electrolyte. This model has been used extensively till date and is popularly known as the Newman model. This model was later modified by Lai et al (2011) (Lai & Ciucci, 2011) in which the used Poisson-Nernst-Plank's equation and volume averaging of the Newman's model to get a generalized equation for lithium ion battery electrode. An application of the Newman porous electrode model was performed for graphite/manganese based lithium battery (Doyle, Newman, Gozdz, Schmutz, & Tarascon, 1996) where they validated the mathematical model with experimental results.

One of the earliest works on thermal modelling of battery was done by Bernardi et al (1985) (Bernardi, Pawlikowski, & Newman, 1985). In their work, they developed a set equations defining different heating sources, like reactions, changes in heat capacity, phase change, mixing, electrical work and heat transfer with the surroundings. These equations were used by Thomas et al (2003) (Thomas & Newman, 2003) in which they estimated the heat generation by Li|LiPF6 in ethylene carbonate: dimethyl carbonate|$LiAl_{0.2}Mn_{1.8}O_{4-8}F_{0.2}$ cells and validated using isothermal calorimetry.

Zhang et al (2000) (Zhang, Popov, & White, 2000) developed a simplified mathematical model to represent the lithium intercalation of a single spinel particle as a microelectrode under the stimulus of a cyclic linear potential sweep. They used the open circuit potential for lithium manganese oxide electrode, found by Doyle et al (1996) (Doyle, Newman, Gozdz, Schmutz, & Tarascon, 1996), to predict that peak current densities depend linearly on the scan rate to a certain power with a constant term, which is different from the predicted peak current density for a conventional redox system.

Diffusion induced stress is a crucial cause of concern in lithium battery electrodes. The diffusion of lithium ions into electrodes during charge/discharge cause a concentration gradient due to the inherent diffusivity of the electrode material. This differential concentration causes the lithium enriched domain to expand more than the deficit zone. Wang et al (2002) (Wang, Lee, & Chen, 2002) developed a chemical stress model for a solid and a hollow cylindrical electrode being lithiated. They used chemically driven expansion on an elastic stress equation to get the stresses and substitute them into the Fick's stress modified diffusion equation to get the concentration profile and the stress generated in the electrode. Yang (2005) (Yang, 2005) did a similar analysis in which he developed A new relation between hydrostatic stress and concentration of solute atoms. However, he solved for a thin plate electrode compared to cylindrical model by Wang et al (2002) (Wang, Lee, & Chen, 2002).

Two papers were published by Christensen and Newman in 2006 exploring a detailed mathematical framework. The first paper (Christensen & Newman, Stress generation and fracture in lithium insertion materials, 2006) developed a mathematical model that calculated the volume expansion and contraction and concentration and stress profiles during lithium insertion into and extraction from a spherical particle of electrode material. They derived the maximum stress in the electrode particle based upon the current flux, charging time and diffusion coefficient of the electrode material. In their second paper (Christensen and Newman 2006), they applied their mathematical framework to obtain stress generation in lithium manganese oxide electrode charged along the 4V plateau and phase change along the 3V plateau.

Work by Zhang et al (2007) (Zhang, Shyy and Sastry 2007) represented a similar stress model for spherical and ellipsoidal lithium manganese oxide electrode being intercalated under constant current conditions. They presented a fully three-dimensional simulation of ellipsoidal particles, to systematically study the intercalation-induced stresses developed in particles of various shapes and sizes. Later, they further worked on heat generation in electrode Zhang et al (2008) (Zhang, Sastry and Shyy 2008). They developed a stress and heat generation model for an electrode spinel. The found that resistive heating, among resistive, entropic and heat of mixing, to be the most dominant heating source in battery electrode. Works by Renganathan et al (2010) (Renganathan, Sikha, Santhanagopalan, & White, 2010) and Barai et al (2013) (Barai & Mukherjee, 2013) also do similar work as Zhang et al (2007) (Zhang, Shyy and Sastry 2007) in modelling the DIS, but under different operating conditions. Renganathan et al (Renganathan, Sikha, Santhanagopalan, & White, 2010) also discussed effects of crack closure in a 3D Li ion particle.

Two prominent works by Suo, Pharr and Zhao in 2010 (Hu, Zhao, & Suo, 2010; Zhao, Pharr, Vlassak, & Suo, 2010) have shown the fracture analysis of lithium batteries using the

fracture energy release rate as the criteria. They calculated the stress and energy release due to a surface crack on lithium cobalt oxide and lithium ferrous phosphate particles respectively. A similar crack propagation model was developed by Bhandakkar et al (2011) (Bhandakkar & Gao, 2011). A life prediction model and capacity fade for graphite-lithium ferrous phosphate particles due to solid electrolyte formation was performed by Deshpande et al (2012) (Deshpande, Verbrugge, Cheng, Wang, & Liu, 2012).

Recent research interest in anodic materials for lithium batteries deal with silicon, due to very high energy storage capacity (~3500 mAh/g). Lithiation initiates with the formation of lithiated silicon amorphous shell on the crystalline (c) silicon nanoparticle. The diffusion of lithium is very slow through the c-silicon hence the phase boundary separating the crystalline crore from amorphous shell is extremely sharp (~ 1nm) (Chon, Sethuraman,, McCormick, Srinivasan, & Guduru, 2011). As the lithium diffuses into the particle, the reaction front propagates forward. The surface is assumed to have the highest concentration of lithiated silicon ($Li_{4.4}Si$) while the reaction front has the lowest in the lithiated domain (minimum of $Li_{3.75}Si$). The lithium concentration drops sharply in the reaction zone which is negligibly thick with no lithium in the crystalline silicon core (Baggetto, Danilov, & Notten, 2011). Lithiation of the particle proceeds through progression of the sharp front along the radial direction towards the center and conversion of the whole nanoparticle from c-silicon to amorphous lithiated silicon.

Previous approaches by Zhao et al (2012) (Zhao, et al., 2012) and Pharr et al (2012) (Pharr, Zhao, Wang,, Suo, & Vlassak, 2012) towards mechanical analysis of silicon lithiation have either assumed a perfectly plastic material or elastic perfectly plastic material response for amorphous lithiated silicon in order to accommodate the large volume expansion during lithiation. Xie et al (2016) (Xie, Ma, Wang, Zhou, & Lu, 2016) modeled the lithiated silicon response with a modulus of 80GPa and flow stress of 1GPa in silicon nanowires during

lithiation. The simplification of high elastic modulus and perfectly plastic materials works well for brittle materials. However, the mechanical response of amorphous lithium silicon is not well understood. Nanoindentation tests on amorphous silicon have reported an elastic modulus within 8 – 12GPa (Berla, Lee, Cui, & Nix, 2015). While experiment based on tensile testing reveal the flow stress to be between 500 – 750MPa (Kushima, Huang, & Li, 2012). The large discrepancy between the modelling assumptions and experimental results on mechanical response limit the understanding of silicon response to lithiation. As a first step towards design of advanced energy systems, it is important to understand how the mechanical response of amorphous phase can influence the stress fields and fracture response of nanoparticles during lithiation.

CHAPTER 3. VARIABLE ELASTIC MODULUS ON FRACTURE CHARACTERISTIC OF LITHIATED SILICON

Mathematical Formulation

A lithium silicon battery system (schematically shown in Figure 2(a)) stores and discharges electrical energy through the exchange of lithium ions between the electrodes. The cell charges with lithium ions moving out of the cathode (metal oxide of lithium) and reacting with silicon at the anode to form lithiated silicon.

$$LiMO_2 \xrightarrow{Cathode} Li_{1-x}MO_2 + xLi^+ + xe^- \quad [1]$$

$$xLi^+ + xe^- + Si \xrightarrow{Anode} Li_xSi \quad [2]$$

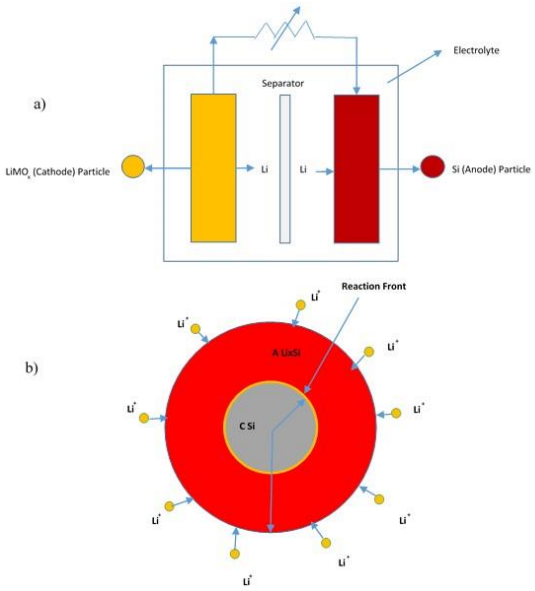

Figure 2. a) Schematic of lithium-silicon battery; b) Diffusion-Reaction Mechanism of lithium during charging in silicon nanoparticle.

Reactive Diffusion Model

Lithium transport in the nanoparticle was modeled based on the following assumptions: 1) Steady state diffusion was considered in amorphous shell, 2) Diffusion in the crystalline core

was considered negligible, 3) The reaction front thickness was taken of negligible thickness with a sharp change in concentration across it. The diffusion of lithium in the amorphous shell was solved based on Fick's Second Law of diffusion.

$$\frac{D}{r^2}\frac{\partial}{\partial r}\left(r^2\frac{\partial c}{\partial r}\right)=0 \qquad [3]$$

Where, D is the diffusivity of lithium in amorphous silicon shell, c is the lithium concentration in the shell. The equation was solved using two boundary conditions.

$$-D\left.\frac{\partial c}{\partial r}\right|_{r=R}=J_b \qquad [4]$$

$$c\big|_{r=R}=c_b \qquad [5]$$

Where, J_b is the surface flux of lithium ion and c_b is the lithium concentration on the surface of the anode particle. The reaction is carried forward by lithium reacting with crystalline silicon at the reaction front. A mass balance was satisfied across the boundary of the reaction front.

$$-D\left.\frac{\partial c}{\partial r}\right|_{r=a}=k(c\big|_a-c_0) \qquad [6]$$

Where, k is the rate of reaction, c_a is the concentration of lithium at the reaction front and c_0 is the minimum possible concentration of lithium in amorphous silicon. The surface concentration was considered to change linearly as the reaction front moves in.

$$c_b=c_{\max}-y(c_{\max}-c_0) \qquad [7a]$$

$$y=\frac{a}{R} \qquad [7b]$$

Where, y is the location of the reaction front and it moves from 0 towards 1, R is the particle radius and a is the crystalline silicon radius.

Elasto-Plastic Mechanics Model

An elasto-plastic stress model was used to determine the stress field generated by the lithium concentration gradient in the particle. The elastic part was driven by expansion stresses due to concentration difference. When the yield criterion was attained, perfect plastic expansion was assumed to express the plastic deformation of the electrode particle. Stress field in the particle satisfied the stress equilibrium:

. $$\frac{\partial \sigma_r}{\partial r} + 2\frac{\sigma_r - \sigma_\theta}{r} = 0 \qquad [8]$$

Where σ_r and σ_θ are the radial and hoop stress in the spherical particle. In the elastic domain, the strain produced is based on the expansion due to lithium diffusion.

$$\varepsilon_{ij}\Big|^{el} = \frac{1}{E}\Big[(1+\nu)\sigma_{ij} - \nu\sigma_{kk}\delta_{ij}\Big] + \frac{\tilde{c}\Omega}{3}\delta_{ij} \qquad [9]$$

Where, $\tilde{c}$ is the concentration difference with respect to initial concentration. The yield criteria used to detect the plastic domain was based upon the yield stress (σ_{yield}).

$$\left|\sigma_\theta - \sigma_r\right| \le \sigma_{yield} \qquad [10]$$

The following boundary conditions were used to merge the free expanding core to the elastic (el) domain and the latter with the plastic (pl) domain.

$$\left.\frac{\partial \sigma_r^{el}}{\partial r}\right|_a = 0 \qquad [11]$$

$$\sigma_r^{el} = \sigma_r^{pl}\Big|_{r_p} \qquad [12]$$

$$\sigma_r^{pl}\Big|_R = 0 \qquad [13]$$

The surface of the particle was considered traction free. Computed stress fields were used to determine the crack driving force for radial cracks. The stress intensity factor (K_I) was calculated using the weight function theory. This model compared the electrode spherical

particle with an equivalent cuboid having a semi-circular crack under the same stress conditions as the particle.

$$K_I = \frac{E}{K_{ref}(1-\nu^2)} \int_0^a \sigma_\theta(x) m(x,a) dx \quad [14]$$

$$m(x,a) = \frac{\partial}{\partial a}\left[\frac{\sigma_{\theta \max}(1-\nu^2)}{E\sqrt{2}} \left\{ 4F\left(\frac{a}{l}\right)\sqrt{a}\sqrt{a-x} + G\left(\frac{a}{l}\right)\frac{(a-x)^{\frac{3}{2}}}{\sqrt{a}} \right\} \right] \quad [15]$$

Where, K_{ref} is the reference stress intensity, E is the elastic modulus, υ is the Poisson's ratio and m(x,a) is the weight function. The stress intensity factors were compared to fracture toughness of amorphous lithiated silicon, estimated using the following formulation.

$$K_{1c} = \sqrt{2E\gamma} \quad [16]$$

Where γ is the surface energy of the material. The governing equations were non-dimensionalized using:

$$\sigma_n = \frac{\sigma}{\sigma_{yield}} \quad [17a]$$

$$K_n = \frac{K_I}{K_{1c}} \quad [17b]$$

Table 1. Lithiated Silicon electro-chemical properties

Property	Value	Reference
Diffusivity (m^2/s)	10^{-16}	(Ma, et al., 2015)
Reaction Rate (m/s)	2.54×10^{-9}	(Cui, Gao, & Qu, 2013)
Maximum Concentration (mol/m^3)	0.36×10^{6}	(Chen, et al., 2014)
Molar Volume (m^3/mol)	1.2×10^{-5}	(Zhao, et al., 2011)
Poisson's Ratio	0.30	(Huang, Fan, Li, Zhang, & Zhu, 2013)
Surface Energy (J/m^2)	0.85	(Tilli, et al., 2015)
Young's Modulus of c-silicon (GPa)	190.00	(Hopcroft, Nix, & Kenny, 2010)
Radius of Particle (nm)	200, 450	

Table 2. Elastic Moduli and Yield Strength for Lithiated Silicon

	Young's Modulus (GPa)	Yield Strength (Berla, Lee, Cui, & Nix, 2015) (MPa)
1	80 (Pharr, Zhao, Wang,, Suo, & Vlassak, 2012)	720
2	35 (Qi, Hector, et al., 2014)	720
3	12 (Berla, Lee, Cui, & Nix, 2015)	720

The normalized equations were solved for a silicon nanoparticle using Mathematica 10.4 (Wolfram Research, 2016). The mechanical and electrochemical properties listed in Table 1 were used to describe the mechanical and lithiation response crystalline silicon. In addition,

the stress and fracture response were computed using three different elastic moduli for lithiated silicon as listed in Table 2. First set of values corresponds to values that have been extensively used in literature considering brittle behavior of silicon. Second set of values were considered from former calculations using Density Functional Theory. The final set corresponds to values reported based on tensile and creep tests of silicon nanowires.

Results and Discussion

The mathematical model was solved for a silicon nanoparticle with different mechanical properties. The selection of a more practical output is then verified by varying the particle radius to match with TEM results. The model has been developed in Mathematica 10.4.

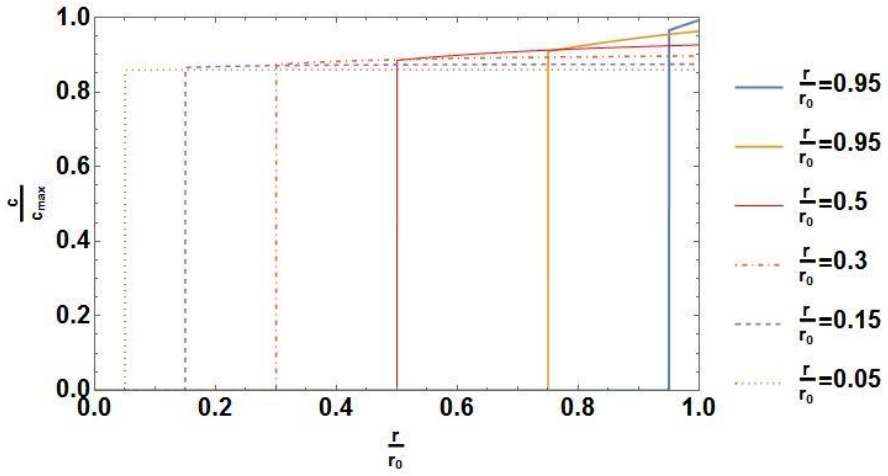

Figure 3. Normalized concentration vs normalized radius variation at different stages of penetration of reaction front into silicon particle.

The concentration profiles of lithium in the amorphous silicon shell computed for different penetration depths of the reaction front in a 200nm particle are plotted in Figure 3. The propagation of the reaction front depended on the rate of reaction. The particle started with zero lithium concentration (t = 0 sec). As the lithium starts reacting with the crystalline silicon, it converted in to amorphous lithiated silicon. The crystalline and amorphous layers were separated by a sharp reaction front. The lithium kept diffusing into the amorphous phase from

the electrolyte and pushed the front into the particle. As the amorphous phase expanded, it provided the saturated lithium in the outer shell more space to diffuse. This caused the slope of the concentration to gradually flattens with the increment of the reaction front. The steady state diffusion process means that the concentration profile does not grow with time. So, the flux of lithium was not considered constant and taken to reduce as the front propagates towards the center of the spherical particle (r = 0).

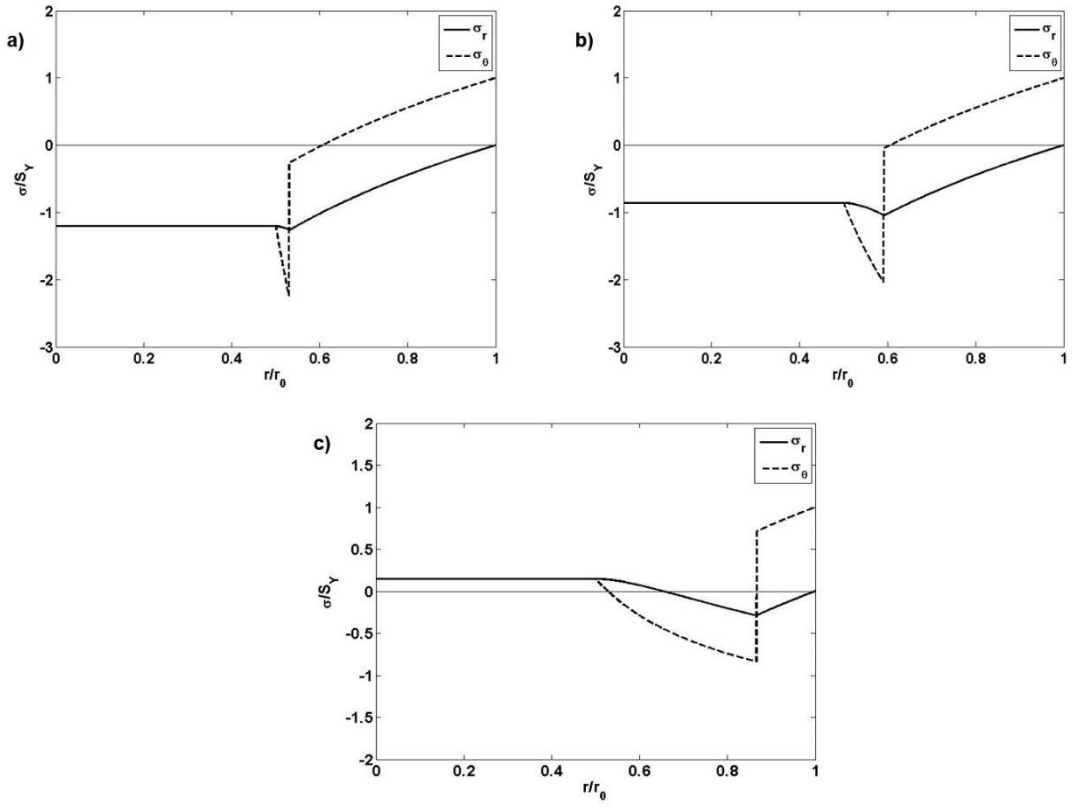

Figure 4. Normalized stress (radial and hoop) vs normalized radius for a 200nm particle considering different elastic moduli; a) 80GPa, b) 35GPa, c) 12GPa.

The dimensionless stress (radial and hoop) profile within the particle at 50% reaction through the particle (radius 200nm) corresponding to the three different values of mechanical properties in Table 2 are shown in Figures 4 (a), (b) and (c), respectively. The surface of the nanosphere was considered traction free, i.e. the particle surface expanded freely. Due to the low diffusivity of lithium in c-silicon, the inner crystalline core had minimal lithium concentration. Therefore, the core had no stress gradient as it gets stretched (or compressed)

by the amorphous layers expanding (contracting) during lithiation. In the material near the reaction front, the lithium concentration jumped and rapidly built up. The expansion due to the formation of lithiated silicon is analogous to thermal expansion and the concentration gradient across the reaction front leads to variation in the stress in the amorphous material. The elastic stresses were compressive where the lithium concentration was higher and the stress state move towards tension as the concentration decreases. This occurred because the higher concentration domain wanted to expand but its free expansion was restricted by the zones with lower lithium concentration. The particle expanded elastically till the difference between the radial and hoop stress exceeded the yield strength of the material causing plastic deformation. After the onset of yield, the material expanded through plastic deformation. As lithiated silicon has been modeled as perfectly plastic, the equilibrium and yield criteria determine the stress distribution in the plastically deformed zone. As shown in Figure 4, the thickness of the elastic zone increased from (a) to (c) as lower magnitude of moduli were used in the analysis. More interestingly, lower magnitude of modulus resulted in a fascinating outcome. The core silicon with higher modulus for lithiated silicon (shown in Figure 4(a)) is under compressive stresses because the elastic domain is thin. However, for a lower value of lithiated silicon modulus (shown in Figure 4(c)), the stress distribution results in a larger elastic domain, causing tensile hoop stress in both the core and the plastic domain. The development of tensile stress near the surface and core will cause any surface or internal flaws to open causing the particle to fail during charging. Crack driving forces corresponding to different stress distributions were computed to better understand the fracture behavior of silicon nanoparticles.

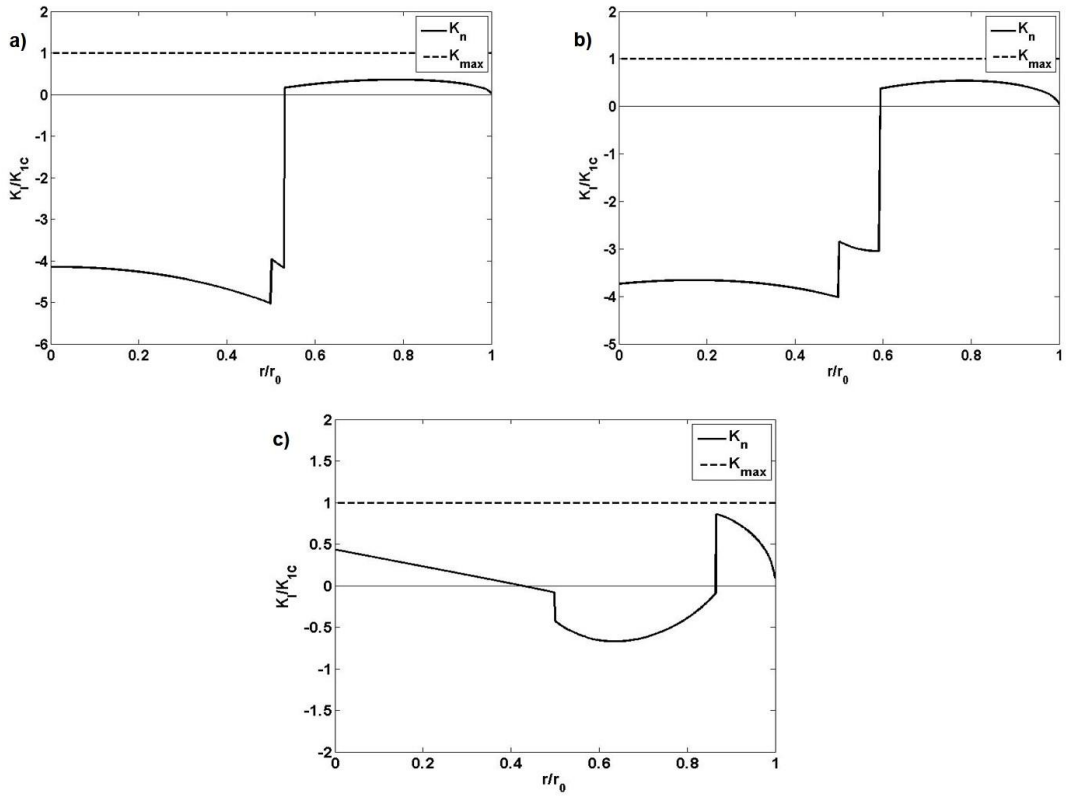

Figure 5. Normalized stress intensity factor vs normalized radius for a 200nm particle with different elastic moduli; a) 80GPa, b) 35GPa, c) 12GPa.

Computed stress intensity factors for radial cracks in a 200nm particle with 50% lithiation reaction were plotted as a function of crack length (as shown in Figures 5 (a), (b) and (c)), corresponding to three different elastic moduli shown in Table 2. The stress intensity factors were computed for radial crack emanating from outer surface and growing towards the center based on analysis reported by Woodford et al (Woodford, Chiang, & Carter, 2010). The hoop stress is the stress component will result in opening and propagation of radial cracks in the spherical system. The domains having positive (or tensile) hoop stress are prone to cracking while compressive hoop stress causes crack closure and arrests the crack propagation. All the values are non-dimensionalized to facilitate comparison for three different modulus systems. For Figure 5(a, b) the short cracks on outer surface with a flaw will have positive stress intensity because of positive hoop stress on the particle surface. But as the crack grow towards the center the hoop stresses become compressive and cause crack closure. For the lower elastic modulus

system shown in Figure 4(c), the particle has tensile hoop stress both on the surface and in the core with a domain of compressive stresses in the middle. This gets reflected by the increasing positive K_n (Figure 5(c)) on the surface which dips down to negative as the compressive hoop stress causes crack closure and again becomes positive due to the tension in the particle core. None of the above case studies showed particle failure. In addition, these results suggest that improving the moduli or hardness of the lithiated silicon may improve the fracture response during charging.

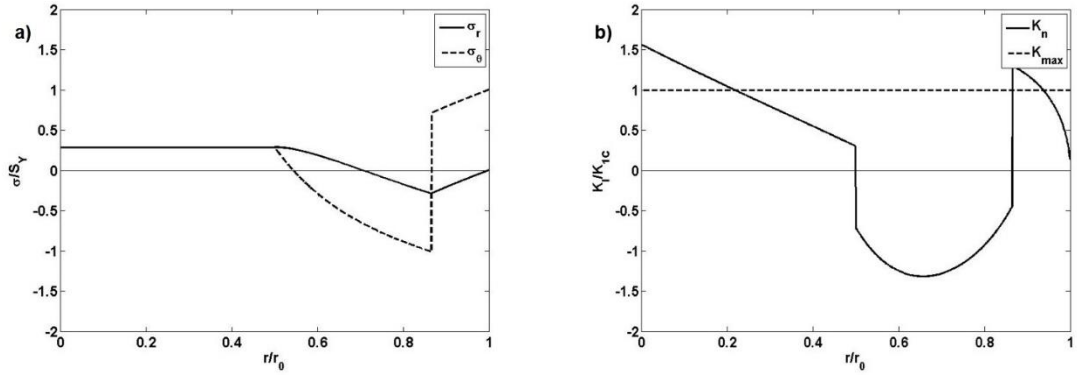

Figure 6. A 450nm particle is considered with elastic modulus of 12GPa; a) Normalized stress (radial and hoop) vs normalized radius, b) Normalized stress intensity factor vs normalized radius.

In order to the investigate the size dependence of fracture response of Si nanoparticles observed by (Liu, et al., 2012), stress distribution and crack driving forces were compute for a particle with radius of 450nm. Figure 6(a) shows the normalized stress state of the particle with lithiated silicon modulus of 12GPa during charging when the reaction front had propagated half way through the material. On comparison with Figure 4(c), the tensile hoop stress in the core was higher in magnitude for the 450nm particle. Figure 6(b) shows the normalized stress intensity for the same particle corresponding to elastic modulus of 12GPa. The crack driving force was found greater than the fracture toughness for cracks near surface (x_n 0.05~0.15) as well as near the core (x_n 0.75~1.00). If there are any flaws in these zones, then they will propagate and fail the particle. These results also explained the sized dependent failure of the silicon particles during charging. Particles smaller than or equal to 200nm have lower stress

distribution and thus the crack driving forces are smaller than the fracture toughness of the particle. As the particle size increases, the magnitude of charging induced stresses as well as the crack driving forces increases and thus may result in failure of larger particle (near or above 450nm).

These results clearly show that accurate characterization of lithiated silicon elastic modulus is important to accurately model the stress development and cracking response of silicon nanoparticles. The results also suggest that increasing the modulus or hardening of lithiated silicon may improve the fracture response of silicon nanoparticles and in turn design of better energy storage materials.

Validation

The case with 12GPa of Elastic Modulus was found similar to experimental observations of charging induced particle fracture from in-situ TEM studies (Liu, et al., 2012). Generally, the positive stress intensity on the surface suggest that surface flaws may propagate to cause fracture. But predictions of higher compressive hoop stress at core for higher elastic moduli in prior mathematical analysis suggested that surface cracks would get arrested near the center of the particle. Experiments by (Liu, et al., 2012) and (Lee, McDowell, Berla, Nix, & Cui, 2012) have shown that silicon particles above 250nm and 350nm undergo complete fracture when charged, irrespective of the charging rate. This observation suggests presence of tensile stresses both near the surface and in the core as the tensile stresses will result in positive crack driving forces and fracture. We found that particles above 400 nm will fail irrespective of the rate of charging.

CHAPTER 4. MATERIAL SELECTION BASED ON THERMAL PERFORMANCE OF LITHIUM-ION BATTERY ELECTRODE MATERIALS

The primary work of a battery is to store energy. A part of this energy is dissipated in the form of heat. The chemo-thermal modelling provided us with a time dependent concentration profile which predicted the diffusion of lithium ions in/out of the electrode particle. The flux of lithium ions occured due to a potential difference across the electrodes when the battery is charged/discharged. The charge transfer led to heat generation in the electrode particle.

Mathematical Formulation

Heat generation in lithium ion batteries can be accounted from several mechanisms. Three dominant heating mechanisms were considered, i.e. polarization (Q_p), joule (Q_j) and entropic (Q_e) heating. There are other heating sources like heat of reaction and heat due to mixing which becomes dominant only at high temperatures leading to thermal runaway. The average heat generated was calculated by volume averaging all the heating sources.

$$\dot{q} = \frac{Q_p + Q_e + Q_j}{V_{par}} \qquad [18]$$

Here, V_{par} is the particle volume. The surface of the electrode particle is exposed to a potential field as per the Butler-Volmer kinetics. The surface over-potential was found by solving the Butler-Volmer equation:

$$\frac{i}{F} = k_r c_l^{1-b} c_\theta^{1-b} c_s^b \left[\exp\left(\frac{(1-\alpha)F\eta}{RT} \right) - \exp\left(\frac{-\alpha F\eta}{RT} \right) \right] \qquad [19]$$

$$\eta = V_{app} - U_{OCP}(\hat{c}) \qquad [20]$$

Where, c_l is the lithium concentration in electrolyte, c_s is the lithium concentration on the electrode surface and c_θ is the lithium concentration in vacant sites ready for intercalation (c_l-c_s). The rate of reaction for the given material is represented by k_r. The applied voltage (V_{app}) could be calculated for a given material for a given applied current. The open circuit potential (U_{OCP}) is a material property of the electrode and function of lithium concentration.

The polarization heating occurs due to charge accumulation due to the difference between surface overpotential, which is the difference between applied voltage and the open circuit potential. The Butler-Volmer reaction rate equation was used to calculate the overpotential and consequently the applied voltage for the battery under a constant current condition.

$$Q_p = I_{app}\eta \quad [21]$$

$$I_{app} = iA_{par} \quad [22]$$

Where the applied current (I_{app}) is defined as the current flux (i) on the electrode times the surface area of the particle (A_{par}). The entropic heating results from the change of the open circuit potential with temperature. It occurs due to free energy change in the electrode particle. The entropic heating was accounted based on the following formulation:

$$Q_e = I_{app}T\frac{\partial \bar{U}_{OCP}}{\partial T}(\hat{c}) \quad [23]$$

Where the differential of U_{OCP} with respect to T is experimentally found for most battery materials. Joule heating occurs due to the internal resistance of the electrode material against the flow of charge through the battery.

$$Q_j = I_{el}{}^2 R_{\text{int}}\left(\frac{V_{par}}{V_{el}}\right) \quad [24]$$

$$I_{el} = iA_{el} \quad [25]$$

The joule heating was found using the total current (I_{el}) flowing across a rectangular electrode surface (A_{el}) and converted to heat generation by a particle using volume average method. The heat due to mixing of lithium ion into the electrode particle were assumed to be negligible value and no side reaction was considered.

Parametric Analysis

The heat generation in the lithium battery electrode was found due to three primary heat generation sources, i.e. polarization, entropic and joule. Each of these heat sources are dependent on material properties like electrode capacity, diffusivity, reaction rate, entropic capacity, internal resistance, etc. as well as physical conditions like diameter of particle, charging rate and state of charge. Literature has shown that different materials intercalate differently and some undergoing phase transformation while others by reaction. However, the diffusion based chemical transport is common in all battery materials. Since the fundamental mechanism is the same, it is convenient to compare every possible candidate material on the basis of heat generation and.

Figure 7. Material Selection process representation.

A parametric analysis was based on four fundamentals. Figure 7 shows the process followed in development of the material indices. First step was the selection of a quantity or parameter that needed to be optimized. Next the governing equation representing the phenomena, like heat generation or diffusion were defined. Then a set of constraints were set by making suitable approximations. Finally, free variables were defined and substituted by the constraint into the parameter to be optimized to derive the indices. It was important to set certain constraints to limit the degree of variability in the material indices. The selection of

constraints allowed comparison on a homogenous basis and also provided flexibility to set certain parameters common for all materials to be compared (Ashby, 2005).

Free Variables and Constants

Constraints allow comparison on a homogenous basis and provides flexibility to set certain parameters common for all materials to be compared. One of the constraints was setting the average non-dimensional concentration profile to a constant. This meant that all electrode particles have been diffused with the same amount of lithium ions.

$$\hat{c}\left(\hat{r}\right) = \frac{c}{c_{\max}} = Cons \qquad [26.a]$$

Another constraint was to either set time for diffusion or radius of particle as a constant. This became slightly challenging as keeping equal radius particle seemed to be a more appropriate decision. However, from an electrochemical perspective, the time required for charging is crucial. The modern trend for charging batteries dictate faster rate of charging, thus making comparison based on equality in temporal coordinates a most more suitable choice.

$$\hat{t} = \frac{tD}{r_o^{\,2}} \qquad [26.b]$$

If the total time required for diffusion is constant, then it can be stated that:

$$r_o \propto \sqrt{D} \qquad [26.c]$$

The temperature of all electrode materials was assumed constant.

Table 3. Thermo-Chemical material properties for lithium-ion battery electrode materials

Properties	$LiMn_2O_4$	$LiCoO_2$	$LiFePO_4$	Li_xC	Li_xSi	Li_xTiO_2 (LTO)
D (m^2/s)	7.08×10^{-15}	1.00×10^{-13}	7.96×10^{-16}	3.90×10^{-14}	1.00×10^{-16}	6.8×10^{-15}
ρ (kg/m^3)	4100.00	5030.00	3600.00	2100.00	2328.00	3510.00
α_{th} (mAh/g)	148.00	166.00	170.00	372.00	4200.00	175.00
c_{max} (mol/m^3)	2.29×10^{4}	4.99×10^{4}	2.12×10^{4}	3.05×10^{4}	8.87×10^{4}	5.00×10^{4}
k_r ($m^{5/2}/mol\text{-}m^3$)	1.90×10^{-9}	5.18×10^{-9}	3.12×10^{-12}	5.03×10^{-11}	5.00×10^{-10}	5.00×10^{-13}
dU/dt (mV/K)	0.50	0.25	0.30	0.14	0.50	0.10
R_{int} (mΩ)	63.00	38.40	20.00	1430.00	1620.00	1.00
k_{th} (W/m-K)	0.80	0.32	2.70	80.00	4.50	1.04

Table 3 data were taken from (Berla, Lee, Cui, & Nix, 2015; Kushima, Huang, & Li, 2012; Ma, et al., 2015; Chen, et al., 2014; Zhao, et al., 2011; Qi, Hector, James, & Kim, 2014; Qi, Hector, James, & Kim, 2013; Renganathan, Sikha, Santhanagopalan, & White, 2010; Bach, Pereira-Ramos, Baffier, & Messina, 1992; Zhang, Popov, & White, 2000; Satyavani, Kiran, Kumar, Kumar, & Naidu, 2016; Bazinski & Wang, 2014; Al Hallaj, Venkatachalapathy, Prakash, & Selman, 2000; Takahashi & Srinivasan, 2015; Zhu & Wang, 2010; Thomas & Newman, 2003; Saito, Shikano, & Kobayashi, 2013; Xu, Zhang, & Li, 2015; Chen, et al., 2015; Lundgren, 2015; Farkhondeh Borazjani, 2016; Hellwig, Sörgel, & Bessler, 2011; Gotcu & Seifert, 2016; Kam & Doeff, 2012; Julien, Mauger, Zaghib, & Groult, 2014). Most of the data have been obtained from previous experiments, mathematical models or interpolated based on a good approximation from the behavior of the material.

Polarization Index

The first heat source in lithium ion electrodes was due to the difference between applied voltage and open circuit potential when current flows through the electrode.

$$\eta = \frac{RT}{\alpha F} a\sinh\left(\frac{i}{Fkc_{\max} c_l^{1-\alpha}\hat{c}^{\alpha}\hat{c}^{1-\alpha}}\right) \quad [27]$$

$$\eta = A_1 a\sinh\left(\frac{A_2\rho\alpha_{th}\sqrt{D}t_0}{kc_{\max}}\right) \quad [28]$$

Where, A1 and A2 are constants. The diffusion time constant (t_0) was assumed to be equal to one.

$$Q_p \propto A_3\left(\rho\alpha_{th}\sqrt{D}\right) a\sinh\left(\frac{A_2\rho\alpha_{th}t_0\sqrt{D}}{kc_{\max}}\right) D \quad [29]$$

$$M_p = \min\left[\left(\rho\alpha_{th}\right) a\sinh\left(\frac{\rho\alpha_{th}t_0\sqrt{D}}{kc_{\max}}\right) D^{\frac{3}{2}}\right] \quad [30]$$

The diffusion coefficient arose from the particle area was multiplied with the current flux to get the total current going into the particle. The constant A2 was ignored as its effect was negligible.

Entropic Index

The second heat generation source was due to entropic changes to the over potential in the battery module. A similar analysis was applied to attain a merit index to minimize the entropic heating term.

$$Q_e \propto A_4\left(\rho\alpha_{th}\sqrt{D}\right)\frac{\partial\bar{U}_{OCP}}{\partial T} D \quad [31]$$

$$M_e = \min\left[\left(\rho\alpha_{th}\right)\frac{\partial\bar{U}_{OCP}}{\partial T} D^{\frac{3}{2}}\right] \quad [32]$$

Joule Index

The joule heating was considered to arise due to the internal resistance of the electrode and therefore was material dependent.

$$Q_j \propto A_5 \left(\rho \alpha_{th} \sqrt{D}\right)^2 R_{\text{int}} D^{\frac{3}{2}} \quad [33]$$

$$M_j = \min\left[\left(\rho \alpha_{th}\right)^2 R_{\text{int}} D^{\frac{5}{2}}\right] \quad [34]$$

The diffusion coefficient raised to five half power in the above equation occurred due to the volume scaling in joule heating.

Thermal Diffusion Index

Thermal diffusion ability was another way to categorize materials which are generating heat. A good choice of electrode material should be able to dissipate heat quicker than other possible candidates. The heat dissipation equation was based on a source term.

$$\rho c_p \frac{\partial T}{\partial t} = k_{th} \frac{1}{r^2} \frac{\partial}{\partial r}\left(r^2 \frac{\partial T}{\partial r}\right) + \dot{q} \quad [35]$$

Normalizing this Equation [35] pushed all material dependence to the source term.

$$\frac{\partial \theta}{\partial \hat{t}} = \frac{1}{\hat{r}^2} \frac{\partial}{\partial \hat{r}}\left(\hat{r}^2 \frac{\partial \theta}{\partial \hat{r}}\right) + \frac{\dot{q} r^2}{k_{th} \theta_{\max}} \quad [36]$$

Considering all particles generated the same amount of heat and replacing the free variable, r, the normalized heat generation term was minimized for lower temperature variation.

$$M_d = \min\left[\frac{D}{k_{th}}\right] \quad [37]$$

Results and Discussion

The thermo-chemical model was developed for a generalized material candidate for lithium ion battery electrodes. Six different materials were selected to be compared based on their heat generation ability and thermal performance. The materials were lithiated by ignoring

any phase transformation during lithiation process. The power released as heat was estimated for an entire electrode of equal diffusion time in all materials to provide a uniformity of comparison. The lithium concentration required to solve the heat generation model was considered equal and constant for all materials. The partial differential equations were solved using Euler Explicit scheme. All calculations were performed on Matlab platform (Guide, 1998).

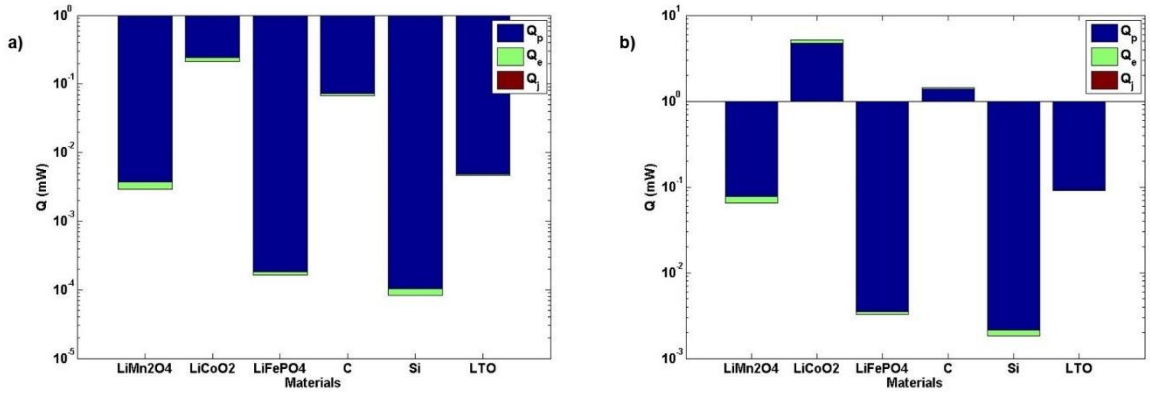

Figure 8. Heat Generation in electrode for cathode and anode materials at different rate of charging; a) 1 C, b) 15 C.

Figure 8 shows the total heat generated by different battery materials at 1 C and 15 C charging rates. The calculation was based upon an averaged heating from the three mechanisms. The temperature for the above calculations is maintained at 298 K and the particle was lithiated for 2000 sec for all systems. The radius of each electrode material was selected based on equality of diffusion time. The electrolyte lithium concentration (c_l) was assumed to be constant for all battery systems and equal to 1000 mol/m^3. A common trend for both the plots was observed based upon the magnitude of heat generation. Three cathode and anode materials were selected. Amongst the three cathode materials, lithium cobalt oxide showed the highest heat generation during lithiation while lithium ferrous phosphate showed the lowest. This means that cobalt oxide batteries have the potential to generate more heat during charging at the same rate when compared to other cathode materials while ferrous phosphate shows the

least heating tendency. Among the anode materials, lithium titanate and silicon showed excellent thermal characteristics as they generated the least heat for the same diffusion rate.

It was interesting to observe the shift in the proportions between the different heating mechanisms as the charging rate increases from 1 C to 15 C. For lower charging rates, entropic heating was significantly contributing with polarization heating. As the charging rate (current flux) increased, there was a transition occurring towards a dominant polarization heating because of the stronger influence of the over potential at higher current flux. With the increase in charging rates, the point of focus shifted towards the minimization of polarization heating component.

The predictions for heat generation requires vast data from experimentation and therefore it is less practical to conduct a complete thermal modelling when deciding a new material. It is important to study material properties governing the thermal aspect of batteries. For selection of materials without actual testing, it is crucial to have a set of material indices to compare them with existing material pool and justify their viability.

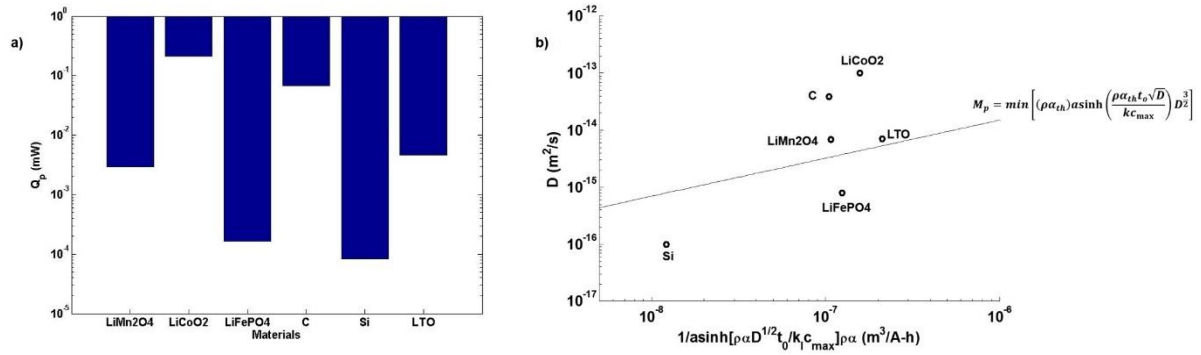

Figure 9. Heat Generation and Material Selection based on Polarization Heating Mechanism; a) Heat Generation, b) Selection based on minimization of Polarization Index.

Figure 9 represents the thermal generation and material selection based on polarization heating in cathode and anode materials for lithium-ion batteries. The objective was to reduce the heat due to the overpotential created during lithiation of the electrode particle. From Figure 8, it was clear that heating due to surface potential difference was the most dominant factor in

heating of the battery. The comparison between the cathode materials showed that lithium ferrous phosphate had the best performance with heat generation several orders of magnitude lower than lithium cobalt oxide. From Figure 9(a) Cobalt oxide based electrodes generate three orders of magnitude more heat than other comparable materials. We believe that there are two primary properties that govern the polarization heating, i.e. density and mass diffusivity. A dense electrode material has a higher ability to store charge for the same capacity. This leads to a higher current absorption ability which is a primary cause of heating in batteries. Moreover, higher mass diffusivity can be related to larger particle radius, under the constraint of uniform diffusion time. Larger particles tend to generate more heat which also adds up to the increase in lithium absorption during lithiation. Lithium cobalt oxide has high density and low capacity amongst the cathode materials which justifies its high polarization heating tendency. From Figure 9(b), materials like lithium ferrous phosphate and silicon were below the minimization line, closely followed by lithium titanate. These materials generate less heat as cathode and anode respectively. The low diffusivity of lithium ferrous oxide means that its particle size would be small for same diffusion time. A similar thought can be applied for the anodic particles. Amorphous silicon has significantly low diffusion coefficient compared to others and thus generates very low polarization heat. For high heat generating materials like lithium cobalt oxide, it is advisable to maintain lower particle diameter in order to reduce the heating tendency. This may be challenging due to manufacturing difficulties, but a trade-off is essential to attain better thermal performance.

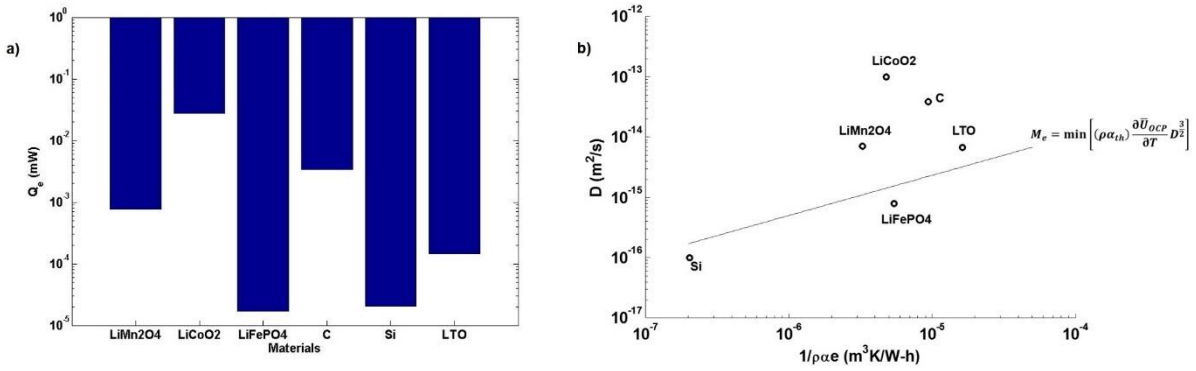

Figure 10. Heat Generation and Material Selection based on Entropic Heating Mechanism; a) Heat Generation, b) Selection based on minimization of Entropic Index.

Merit index comparison based on entropic heating in electrode materials is represent in Figure 10. Entropic heating in a battery occurs due to the entropic changes in the material when it gets lithiated. This index is crucial for lower charging rates (C_{rate}~1-5) and decreases in proportion with increase in current flux. As the material reacts with lithium, its bond structure is altered to accommodate the insertion of the ion. The change in the bond energy and resulting changes in the overall dipole of the material cause energy generation (or absorption) during lithiation/delithiation. Entropic heating and the change of open circuit potential are of major importance as they leads to heat generation and thermal runaway in batteries. It was clear from the merit index minimization (Figure 10(b)) that among the cathode materials, lithium ferrous phosphate showed the lowest entropic heating nature while lithium cobalt oxide produced the highest heat. This index depends on three parameters, i.e. density, diffusion coefficient and entropic potential. The product of the current and entropic potential results in the thermodynamic entropy ($\Delta S=I(dU/dt)$) of the electrode particle. It was very interesting to find that lithium cobalt oxide has slightly lower entropic potential than lithium ferrous phosphate. However, the total entropy change was lower for lithium ferrous phosphate and very high for lithium cobalt oxide. Experiments are performed to improve the entropy based properties of lithium electrode by altering the bond structure to reduce the deformations during lithiation.

Lithium titanate showed better entropic behavior compared to graphite during lithiation. Graphite has higher entropic potential and current characteristics than lithium titanate, thereby the later has lower entropy resulting in lower heating. Silicon has very high entropic potential compared to other materials. This is expected because lithium deforms the maximum during lithiation. However, its entropy change is the least which makes it the best choice from the entropic index consideration. Since entropic heating starts to impact at low charging rates, it is important to find solutions to mitigate the entropy generation in the electrode materials. Doping with some relaxant can be useful technique to reduce the stress on the particle during lithiation.

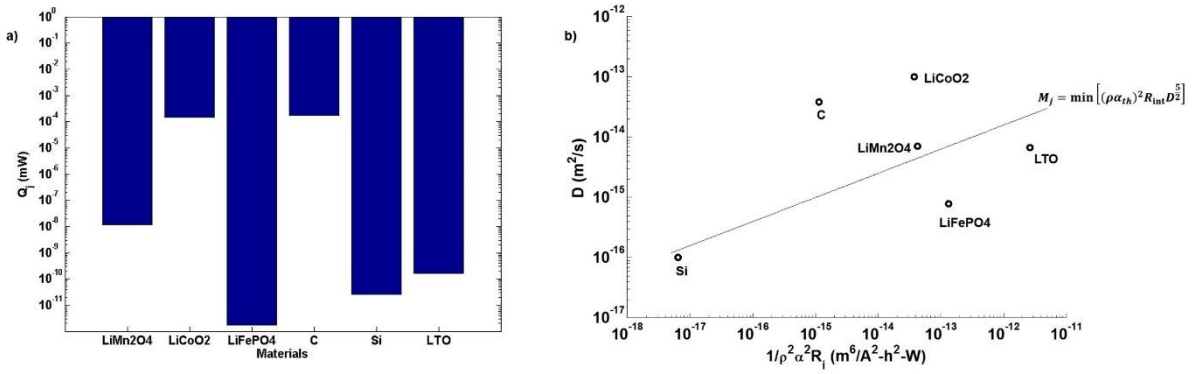

Figure 11. Heat Generation and Material Selection based on Joule Heating Mechanism; a) Heat Generation, b) Selection based on minimization of Joule Index.

The joule heating was categorized based on the current flowing through the electrode and its internal resistance. The Figure 11 shows the merit index to compare cathode and anode materials based on their heat generation due to internal resistance. Internal resistance occurs due to the resistance the lithium ions face from the electrolyte and electrode material system when being charged/discharged. This resistance is proportional to the electromotive force within the battery. From Figure 11(a), lithium cobalt oxide generated the highest heat because of its higher theoretical capacity which allows it to store more current causing the heating problem. Figure 11(b) minimizes the joule index. Among the cathode materials lithium ferrous phosphate has the least internal resistance while lithium titanate has the least resistance among

the anode materials. Silicon very closely follows lithium titanate in the above criterion making it a suitable replacement, capable of generating low resistive heat.

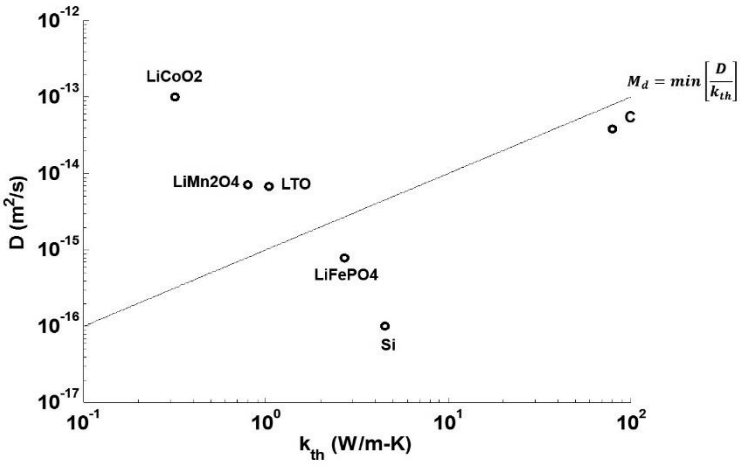

Figure 12. Material Selection based on minimization of Diffusion Index.

All these merit indices are useful in classifying and choosing candidate materials for electrode having lower heat generation characteristics. However, with the present trend of faster charging, all battery materials are expected to face the challenge of over-heating. This has caused many cases of accident and injury due to battery explosion. Therefore, it is necessary that the electrode materials should have excellent thermal diffusion characteristics to mitigate such conditions. The Figure 12 compares the materials based upon their thermal diffusive ability. This merit index assumed that all candidate materials generate the same volumetric heat generation and compares them based upon their thermal stability. A material having smaller radius (or diffusivity) and higher thermal conductivity was a great candidate for this index. Comparing the different cathode materials, lithium ferrous phosphate has the highest (by one order of magnitude) thermal conductivity and lowest mass diffusivity. This meant that a small lithium ferrous phosphate particle had the best ability to diffuse heat, making it suitable for fast charging batteries. Lithium cobalt oxide has the lowest thermal conductivity and high mass diffusivity making it a poor choice for thermally stable material. For the anode materials, graphite has the highest thermal conductivity. However, higher diffusivity (meaning larger

particle size from constraint) made it slightly poor if not equivalent when compared to silicon on the merit index plot. Lithium titanate, which is a promising material based on the heat generation based indices, showed very poor heat diffusion characteristics.

Merit indices based on polarization, entropic and joule heating characteristically showed that lithium ferrous phosphate is the best material for lowest thermal generation. Lithium cobalt oxide is one of the most commonly used battery material for cathode because of it large charge storing capacity. The high heating problem in lithium cobalt oxide can be mitigated by manufacturing smaller sized cobalt oxide particles. Similarly, silicon was found to be the best choice for anode materials. It has excellent thermal diffusion ability and low thermal generation with high capacity. The only drawback for silicon is due to its tendency to plastically deform and it reacts with lithium and generates heat of reaction during the first cycle. However, silicon has no other drawbacks.

Validation

The results have been validated from the experiments conducted by Joachin et al (2009) (Joachin, Kaun, Zaghib, & Prakash, 2009). According to their paper, lithium ferrous phosphate has higher thermal stability at higher temperatures as compared to other oxide electrodes. The work by Viswanathan et al (2010) (Viswanathan, et al., 2010) stated that lithium cobalt oxide has a very large entropic change contributing to high heat generation conditions under charging. Similarly, graphite, silicon and titanium oxide have been selected for the study as anodic materials. The merit indices showed that graphite generated the most heat amongst all anode materials, while silicon and lithium titanate had the least thermal contribution. This has been validated from Viswanathan et al (2010) (Viswanathan, et al., 2010), which compared graphite with lithium titanate and establishes the better thermal performance of lithium titanate over graphite electrodes.

CHAPTER 5. CONCLUSION AND FUTURE SCOPE

Summary and Conclusion

Two research works were established based on the thermo-mechanical modelling of lithium battery systems. The first work dealt with elasto-plastic stress and fracture analysis of silicon electrode during first cycle charging. The influence of elastic modulus and yield strength of lithiated silicon on the stress and fracture response of silicon nanoparticles during charging was investigated. An elasto-plastic stress analysis coupled with steady state diffusion was utilized to determine the stress distribution in silicon particle during charging. Computed stress fields were utilized to determine the crack driving force for radial cracks. Different elastic moduli were considered for lithiated silicon and the numerical results indicated that numerical predictions corresponding to lower elastic moduli could accurately capture the experimentally observed size dependence fracture of silicon particles. These results showed that lower modulus of amorphous lithiated silicon led to development of tensile hoop stresses both on the surface and in the core regions of the silicon particles and thus enhanced the crack driving forces leading to its fracture. Beyond a certain critical radius (about 450nm) a large portion of the particle was affected by stress intensity above critical value predicting failure. These results emphasize the importance of accurate characterization of the mechanical response of amorphous lithiated silicon. Furthermore, the results suggest that hardening of particle to increase its elastic modulus would lead to higher critical stress intensity and lower tendency to have a tensile core. This would prevent crack propagation throughout the material.

The second work demonstrated an innovative approach towards comparison of different electrode materials for a lithium ion battery based upon their thermal performance and stability. The paper was based on the development of a heat generation model from a thermo-chemical diffusion model. Three mechanism of heat transfer were considered, i.e. polarization, entropic

and joule heat, to attain the net heat transfer. Six different materials were selected, three for cathode and anode. Four merit indices were created of which three were used to compare the materials based on the minimization of heat generation and one the last based on their ability to quickly diffuse heat. We conclude that lithium ferrous phosphate is the best candidate for cathode, having minimum heat generation among all three mechanisms and best thermal diffusive performance. Among the anode silicon showed least heat generation and best thermal diffusion characteristic. These materials could be considered as excellent candidates for high speed charging systems. However, materials like lithium cobalt oxide (cathode) and graphite (anode), which are the most commonly used as electrode materials for lithium ion batteries had the worst thermal performance. They generated huge amounts of heat by all the calculated mechanisms and had very poor thermal diffusion ability. It was also found that polarization heating becomes dominant with at high charging rates. To mitigate the problem of high heat generation, it is advisable to reduce the particle size. Another solution is to dope the materials with some relaxing molecule. This would reduce the bond strain due to deformation during lithiation, thereby lowering the entropy generated in the process. Particle size optimization and chemical structure modifications seems to be a few plausible options for improving materials having poor thermal. We believe that the search for new materials would be greatly aided by the comparing them with existing materials based on these material indices.

Future Work

The stability analysis and mitigating the problem of thermal runaway in lithium ion batteries is our current target. The recent events of battery explosion (even after stringent quality inspection) have created a sense of trepidation towards the commercial use of lithium ion batteries. The failure of past numerical models in predicting thermal instability beckons for a novel approach towards instability predictions in li-ion battery. Data driven approach, modelled and investigated by (Chandra, Kar, Wu, Hall, & Gillette, 2015), could be an approach

to qualitatively predict the onset of instability in battery modules. These outcomes validate the accuracy of this DDP methodology and thereby would be a great tool in instability prediction for batteries with different design basis and operating under variable charging conditions. The project targets to perform a Data Driven Prognosis (DDP) algorithm for commercially used manganese/graphite lithium battery having different geometric design, e.g., cell phone based design and aircraft based design. Different operating conditions of current and equivalent voltage will be taken as input for this algorithm. The output will predict the onset of instability for the battery cycling over different temporal scales. Based on the outcome of the DDP model, a numerical scheme will be created using linear perturbation theory including convective boundary conditions and experiment based thermal dependency of material properties of the above-mentioned battery. All heating sources previously modeled will be considered in the perturbation theory to quantifiably establish the optimum design parameters which would avoid thermal instability under given operating conditions. Based on the successful data-driven and numerical analysis for the battery, the project may incorporate an experimental validation of the results and attempt to simulate similar stability predictions and design scheme for silicon based lithium battery, which is one of the cutting-edge technology in li-ion research.

Broad Impact

This project will greatly benefit the battery industry targeting lithium ion and other rechargeable batteries for higher energy storage applications. The stability model will generate parameters and indices which govern the thermal stability of electrode materials. Newer battery materials, like solid state electrolyte and non-stoichiometric hybrids of existing materials, could be parameterized and compared using these indices. The battery dimensions could be predefined based on the expected battery performance to avoid the hazards of thermal runaway. The analysis of DDP to lithium silicon battery would allow a detailed analysis towards the thermal stability of this new battery technology. A good perturbation model for such a system

would be promote a safe research and development in this field without the problem of overheating. Since, silicon systems are a promising candidate for future lithium batteries and great for high energy storage applications like transportation, its stability is crucial for the safety of everyone.

REFERENCES

Al Hallaj, S., Venkatachalapathy, R., Prakash, J., & Selman, J. R. (2000). Entropy changes due to structural transformation in the graphite anode and phase change of the LiCoO2 cathode. *Journal of the Electrochemical Society, 147*(7), 2432-2436.

Armand, M., & Tarascon, J. M. (2001). Issues and challenges facing rechargeable lithium batteries. *Nature, 414*(6861), 359-367.

Ashby, M. F. (2005). *Materials selection in mechanical design.* Cambridge University Press.

Bach, S., Pereira-Ramos, J. P., Baffier, N., & Messina, R. (1992). Thermodynamic data of electrochemical lithium intercalation in LixMn2O4. *Electrochimica acta, 37*(7), 1301-1305.

Baggetto, L., Danilov, D., & Notten, P. H. (2011). Honeycomb-Structured Silicon: Remarkable Morphological Changes Induced by Electrochemical (De) Lithiation. *Advanced Materials, 23*(13), 1563-1566.

Barai, P., & Mukherjee, P. P. (2013). Stochastic analysis of diffusion induced damage in lithium-ion battery electrodes. *Journal of the Electrochemical Society, 160*(6), A955-A967.

Bazinski, S. J., & Wang, X. (2014). The influence of cell temperature on the entropic coefficient of a lithium iron phosphate (lfp) pouch cell. *Journal of The Electrochemical Society, 161*(1), A168-A175.

Berla, L. A., Lee, S. W., Cui, Y., & Nix, W. D. (2015). Mechanical behavior of electrochemically lithiated silicon. *Journal of Power Sources, 273*, 41-51.

Bernardi, D., Pawlikowski, E., & Newman, J. (1985). A general energy balance for battery systems. *Journal of the electrochemical society, 132*(1), 5-12.

Bhandakkar, T. K., & Gao, H. (2011). Cohesive modeling of crack nucleation in a cylindrical electrode under axisymmetric diffusion induced stresses. *International Journal of Solids and Structures, 48*(16), 2304-2309.

Chandra, A., Kar, O., Wu, K. C., Hall, M., & Gillette, J. (2015). Prognosis of anterior cruciate ligament reconstruction: a data-driven approach. *The Royal Society, 471*(2176).

Chang, J., Huang, X., Zhou, G., Cui, S., Hallac, P., Jiang, J., . . . Chen, J. (2014). Lithium-Ion Batteries: Multilayered Si Nanoparticle/Reduced Graphene Oxide Hybrid as a High-Performance Lithium-Ion Battery Anode. *Advanced Materials, 26*(5), 665-665.

Chen, L., Fan, F., Hong, L., Chen, J., Ji, Y. Z., Zhang, S. L., . . . Chen, L. Q. (2014). A phase-field model coupled with large elasto-plastic deformation: application to lithiated silicon electrodes. *Journal of The Electrochemical Society, 161*(11), F3164-F3172.

Chen, M., Sun, Q., Li, Y., Wu, K., Liu, B., P. P., & Wang, Q. (2015). A thermal runaway simulation on a lithium titanate battery and the battery module. *Energies, 8*(1), 490-500.

Chon, M. J., S. V., McCormick, A., Srinivasan, V., & Guduru, P. R. (2011). Real-time measurement of stress and damage evolution during initial lithiation of crystalline silicon. *Physical Review Letters, 107*(4).

Christensen, J., & Newman, J. (2006). A Mathematical Model of Stress Generation and Fracture in Lithium Manganese Oxide. *Journal of The Electrochemical Society, 153*(6), A1019-A1030.

Christensen, J., & Newman, J. (2006). Stress generation and fracture in lithium insertion materials. *Journal of Solid State Electrochemistry, 10*(5), 293-319.

Cui, Z., Gao, F., & Qu, J. (2013). Interface-reaction controlled diffusion in binary solids with applications to lithiation of silicon in lithium-ion batteries. *Journal of the Mechanics and Physics of Solids, 61*(2), 293-310.

Deshpande, R., Verbrugge, M., Cheng, Y. T., Wang, J., & Liu, P. (2012). Battery cycle life prediction with coupled chemical degradation and fatigue mechanics. *Journal of the Electrochemical Society*, *159*(10), A1730-A1738.

Doyle, M., Fuller, T. F., & Newman, J. (1993). Modeling of galvanostatic charge and discharge of the lithium/polymer/insertion cell. *Journal of the Electrochemical Society*, *140*(6), 1526-1533.

Doyle, M., Newman, J., Gozdz, A. S., Schmutz, C. N., & Tarascon, J. M. (1996). Comparison of modeling predictions with experimental data from plastic lithium ion cells. *Journal of the Electrochemical Society*, *143*(6), 1890-1903.

Ellis, B. L., Lee, K. T., & Nazar, L. F. (2010). Positive electrode materials for Li-ion and Li-batteries. *Chemistry of Materials*, *22*(3), 691-714.

Farkhondeh Borazjani, M. (2016). *Modeling and Characterization of Lithium Iron Phosphate Battery Electrodes.* PhD Thesis, University of Waterloo.

Gotcu, P., & Seifert, H. J. (2016). Thermophysical properties of LiCoO 2–LiMn 2 O 4 blended electrode materials for Li-ion batteries. *Physical Chemistry Chemical Physics*, *18*(15), 10550-10562.

Guide, M. U. (1998). The mathworks. Natick, MA.

Hellwig, C., Sörgel, S., & Bessler, W. G. (2011). A multi-scale electrochemical and thermal model of a LiFePO4 battery. *Ecs Transactions*, *35*(32), 215-228.

Hopcroft, M. A., Nix, W. D., & Kenny, T. W. (2010). What is the Young's Modulus of Silicon? *Journal of microelectromechanical systems*, *19*(2), 229-238.

Hu, Y., Zhao, X., & Suo, Z. (2010). Averting cracks caused by insertion reaction in lithium–ion batteries. *Journal of Materials Research*, *25*(6), 1007-1010.

Huang, S., Fan, F., Li, J., Zhang, S., & Zhu, T. (2013). Stress generation during lithiation of high-capacity electrode particles in lithium ion batteries. *Acta materialia, 61*(12), 4354-4364.

Irfan, U. (2014, 12 18). *How Lithium Ion Batteries Grounded the Dreamliner*. Retrieved from Scientific Amercan: https://www.scientificamerican.com/article/how-lithium-ion-batteries-grounded-the-dreamliner/

Joachin, H., Kaun, T. D., Zaghib, K., & Prakash, J. (2009). Electrochemical and thermal studies of carbon-coated LiFePO4 cathode. *Journal of the Electrochemical Society, 156*(6), A401-A406.

Julien, C. M., Mauger, A., Zaghib, K., & Groult, H. (2014). Comparative issues of cathode materials for Li-ion batteries. *Inorganics, 2*(1), 132-154.

Kam, K. C., & Doeff, M. M. (2012). Electrode materials for lithium ion batteries. *Materials Matters, 7*, 56-60.

Kushima, A., Huang, J. Y., & Li, J. (2012). Quantitative fracture strength and plasticity measurements of lithiated silicon nanowires by in situ TEM tensile experiments. *ACS nano, 6*(11), 9425-9432.

Lai, W., & Ciucci, F. (2011). Mathematical modeling of porous battery electrodes—Revisit of Newman's model. *Electrochimica Acta, 56*(11), 4369-4377.

Lee, S. W., McDowell, M. T., Berla, L. A., Nix, W. D., & Cui, Y. (2012). Fracture of crystalline silicon nanopillars during electrochemical lithium insertion. *Proceedings of the National Academy of Sciences, 109*(11), 4080-4085.

Liu, X. H., Zhong, L., Huang, S., Mao, S. X., Zhu, T., & Huang, J. Y. (2012). Size-dependent fracture of silicon nanoparticles during lithiation. *Acs Nano, 6*(2), 1522-1531.

Lundgren, H. (2015). *Thermal Aspects and Electrolyte Mass Transport in Lithium-ion Batteries*. Doctoral dissertation, KTH Royal Institute of Technology.

Ma, Z. S., Xie, Z. C., Wang, Y., Zhang, P. P., Pan, Y., Zhou, Y. C., & Lu, C. (2015). Failure modes of hollow core–shell structural active materials during the lithiation–delithiation process. *Journal of Power Sources, 2015*, 114-122.

Moynihan, T. (2017, 01 22). *Samsung Finally Reveals Why the Note 7 Kept Exploding*. Retrieved from Wired: https://www.wired.com/2017/01/why-the-samsung-galaxy-note-7-kept-exploding/

Pharr, M., Zhao, K., W. X., Suo, Z., & Vlassak, J. J. (2012). Kinetics of initial lithiation of crystalline silicon electrodes of lithium-ion batteries. *Nano letters, 12*(9), 5039-5047.

Qi, Y., Hector, L. G., James, C., & Kim, K. J. (2013). A preliminary investigation of fracture toughness of Li 7 La 3 Zr 2 O 12 and its comparison to other solid Li-ionconductors. *Materials Letters, 96*, 117-120.

Qi, Y., Hector, L. G., James, C., & Kim, K. J. (2014). Lithium concentration dependent elastic properties of battery electrode materials from first principles calculations. *Journal of The Electrochemical Society, 161*(11), F3010-F3018.

Renganathan, S., Sikha, G., Santhanagopalan, S., & White, R. E. (2010). Theoretical analysis of stresses in a lithium ion cell. *Journal of the Electrochemical Society, 157*(2), A155-A163.

Saito, Y., Shikano, M., & Kobayashi, H. (2013). Heat generation behavior during charging and discharging of lithium-ion batteries after long-time storage. *Journal of Power Sources, 244*, 294-299.

Satyavani, T. V., Kiran, B. R., Kumar, V. R., Kumar, A. S., & Naidu, S. V. (2016). Effect of particle size on dc conductivity, activation energy and diffusion coefficient of lithium iron phosphate in Li-ion cells. *Engineering Science and Technology, an International Journal, 19*(1), 40-44.

Takahashi, K., & Srinivasan, V. (2015). Examination of graphite particle cracking as a failure mode in lithium-ion batteries: a model-experimental study. *Journal of The Electrochemical Society, 162*(4), A635-A645.

Thomas, K. E., & Newman, J. (2003). Thermal Modeling of Porous Insertion Electrodes. *Journal of the Electrochemical Society, 150*(2), A176-A192.

Tilli, M., Motooka, T., Airaksinen, V. M., Franssila, S., Paulasto-Krockel, M., & Lindroos, V. (2015). Handbook of silicon based MEMS materials and technologies. William Andrew.

Viswanathan, V.V., Choi, D., Wang, D., Xu, W., Towne, S., . . . Yang, Z. (2010). Effect of entropy change of lithium intercalation in cathodes and anodes on Li-ion battery thermal management. *Journal of Power Sources, 195*(11), 3720-3729.

Wang, W. L., Lee, S., & Chen, J. R. (2002). Effect of chemical stress on diffusion in a hollow cylinder. *Journal of applied physics, 91*(12), 9584-9590.

Whittingham, M. S. (2004). Lithium batteries and cathode materials. *Chemical Reviews, 104*(10), 4271-4302.

Wolfram Research, I. (2016). Mathematica 10.4. Champaign, Illinois.

Woodford, W. H., Chiang, Y. M., & Carter, W. C. (2010). "Electrochemical shock" of intercalation electrodes: a fracture mechanics analysis. *Journal of the Electrochemical Society, 157*(10), A1052-A1059.

Xie, Z., Ma, Z., Wang, Y., Zhou, Y., & Lu, C. (2016). A kinetic model for diffusion and chemical reaction of silicon anode lithiation in lithium ion batteries. *RSC Advances, 6*(27), 22383-22388.

Xu, W., Zhang, G., & Li, B. (2015). Effects of lithium insertion on thermal conductivity of silicon nanowires. *Applied Physics Letters, 106*(17).

Yang, F. (2005). Interaction between diffusion and chemical stresses. *Materials Science and Engineering: A, 409*(1), 153-159.

Zhang, D., Popov, B. N., & White, R. E. (2000). Modeling lithium intercalation of a single spinel particle under potentiodynamic control. *Journal of The Electrochemical Society, 147*(3), 831-838.

Zhang, X., Sastry, A. M., & Shyy, W. (2008). Intercalation-induced stress and heat generation within single lithium-ion battery cathode particles. *Journal of The Electrochemical Society, 155*(7), A542-A552.

Zhang, X., Shyy, W., & Sastry, A. M. (2007). Numerical simulation of intercalation-induced stress in Li-ion battery electrode particles. *Journal of the Electrochemical Society, 154*(10), A910-A916.

Zhao, K., Pharr, M., Vlassak, J. J., & Suo, Z. (2010). Fracture of electrodes in lithium-ion batteries caused by fast charging. *Journal of Applied Physics, 108*(7).

Zhao, K., Pharr, M., Wan, Q., Wang, W. L., Kaxiras, E., Vlassak, J. J., & Suo, Z. (2012). Concurrent reaction and plasticity during initial lithiation of crystalline silicon in lithium-ion batteries. *Journal of The Electrochemical Society, 159*(3), A238-A243.

Zhao, K., Wang, W. L., Gregoire, J., Pharr, M., Suo, Z., Vlassak, J. J., & Kaxiras, E. (2011). Lithium-assisted plastic deformation of silicon electrodes in lithium-ion batteries: a first-principles theoretical study. *Nano letters, 11*(7), 2962-2967.

Zhu, Y., & Wang, C. (2010). Galvanostatic intermittent titration technique for phase-transformation electrodes. *The Journal of Physical Chemistry C, 114*(6), 2830-2841.